RSC Advances

PAPER

View Article Online
View Journal | View Issue

Cite this: *RSC Adv.*, 2023, **13**, 29023

Density functional theory study of the corrosion inhibition performance of 6-mercaptopurine and 6-thioguanine expired drugs toward the aluminium (111) surface†

Mahmoud A. A. Ibrahim, *[ab] Nayra A. M. Moussa,[a] Amna H. M. Mahmoud,[a] Shaban R. M. Sayed,[c] Peter A. Sidhom,[d] Mohamed K. Abd El-Rahman,[e] Tamer Shoeib *[f] and Lamiaa A. Mohamed[a]

The potentiality of the 6-mercaptopurine (**MP**) and 6-thioguanine (**TG**) expired drugs toward the corrosion inhibition of the aluminium **(Al) (111)** surface was widely investigated using a series of density functional theory (DFT) calculations. A competition between the anti-corrosive features of the studied drugs in the gas and aqueous phases was conducted on both neutral and protonated forms by means of quantum mechanical descriptors. The results of the electrostatic potential analysis demonstrated the prominent nucleophilic nature of the sulfur and nitrogen atoms over the structures of the examined drugs. The frontier molecular orbital theory findings outlined the higher preferability of **TG** over **MP** as a corrosion inhibitor. Upon determining the most beneficial configurations of the **MP/TG**···**Al (111)** complexes, first-principles molecular dynamics simulations were executed. Interestingly, the competence of the **TG** drug in the corrosion inhibition process of **Al (111)** was more extensive than that of the **MP** one, which was confirmed by the interaction energy values of −1.79 and −1.64 eV, respectively. Upon obtaining the relaxed complexes, the effect of the presence of water solvent on the adsorption process was studied. These findings provide a foundation for developing green anti-corrosive inhibitors for the aluminium surface.

Received 1st August 2023
Accepted 20th September 2023

DOI: 10.1039/d3ra04954j

rsc.li/rsc-advances

1 Introduction

Nowadays, aluminium (Al) and its alloys are used worldwide in versatile industrial applications, such as automotive, aerospace, electronics, and transportation, owing to their mechanical strength and economical manufacturing cost.[1,2] It is noteworthy that Al and its alloys possess crucial resistance to atmospheric conditions due to a firm adherent metal oxide film.[3] Nevertheless, Al-based alloys are susceptible to localized attack in corrosive environments, like media containing chloride ions.[4–6] Hydrochloric acid (HCl) is a common solution used for chemical, pickling, and electrochemical etching of Al metal and its alloys.[7,8] Further, the HCl solution is used to remove dust and rust in the metallurgical industries. Additionally, the surface of Al in an aqueous solution forms a compact and robust passive oxide coating. This film dissolves when submerged in HCl solution due to its amphoteric nature, leading to corrosion issues.[8–11] Failures and losses resulting from the corrosion phenomena lead not only to economic problems but also environmental, security, social, and safety issues. Up to now, the investigation of corrosion inhibition of metallic surfaces has triggered much industrial and commercial interest. Indeed, corrosion could not be eliminated, but it could be only minimized by utilizing several methods comprising anodizing and coatings.[12,13]

An innovative anti-corrosive approach is the incorporation of organic inhibitors,[14–19] forming a protective barrier by getting adsorbed on the surface of the metals. Organic compounds containing heteroatoms (*e.g.*, N, S, and O) in a conjugated system show high efficiency toward the corrosion inhibition of metals.[20–22] Notwithstanding, the majority of the above-mentioned compounds are highly expensive and toxic to the environment.[23] In this regard, much scientific interest has been

[a]*Computational Chemistry Laboratory, Chemistry Department, Faculty of Science, Minia University, Minia 61519, Egypt. E-mail: m.ibrahim@compchem.net*
[b]*School of Health Sciences, University of KwaZulu-Natal, Westville Campus, Durban 4000, South Africa*
[c]*Department of Botany and Microbiology, College of Science, King Saud University, P.O. Box 2455, Riyadh 11451, Saudi Arabia*
[d]*Department of Pharmaceutical Chemistry, Faculty of Pharmacy, Tanta University, Tanta 31527, Egypt*
[e]*Department of Chemistry and Chemical Biology, Harvard University, 12 Oxford Street, Cambridge, MA 02138, USA*
[f]*Department of Chemistry, The American University in Cairo, New Cairo 11835, Egypt. E-mail: t.shoeib@aucegypt.edu*

† Electronic supplementary information (ESI) available. See DOI: https://doi.org/10.1039/d3ra04954j

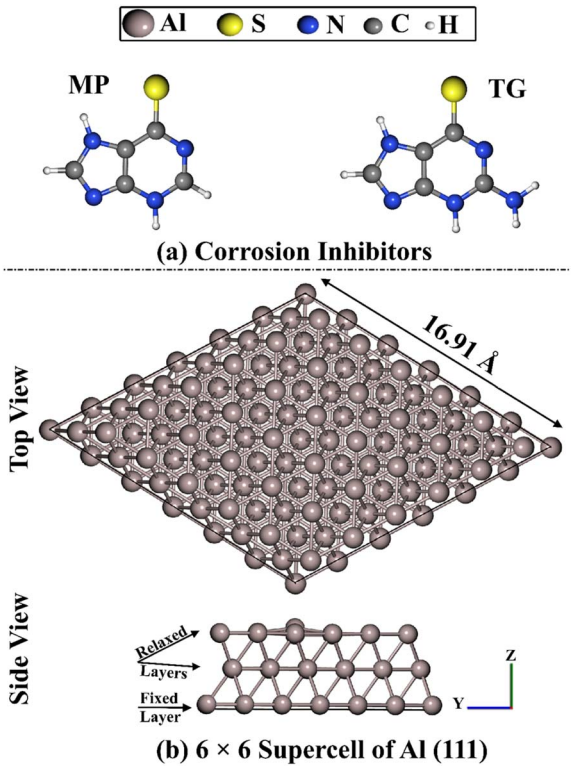

Fig. 1 (a) Illustrative representation for 6-mercaptopurine (MP) and 6-thioguanine (TG) drugs as corrosion inhibitors, and (b) side and top representations of the relaxed 6 × 6 supercell of aluminum Al (111).

directed toward using pharmaceutical vehicles, more specifically expired drugs, as eco-friendly anti-corrosive inhibitors for metals and their corresponding alloys.[24–27]

The investigation of drug inhibitory properties has sparked much interest in recent years. A thorough review documented the potential efficiency of drugs as corrosion inhibitors with limited large-scale practical applications due to the high cost of active substances.[28] In an attempt to avoid the drawback of the high cost of drugs, corrosion research was accordingly directed to explore the applicability of expired drugs as anti-corrosive inhibitors. It was unveiled that the utilization of expired drugs can solve two more crucial issues, including the reduction of drug disposal costs and limiting environmental pollution with drugs.[29]

As crucial N-heterocyclic pharmaceutical compounds, purines and their derivatives were deemed to be potential corrosion inhibitors for metals involving steel,[30–33] aluminium,[34,35] tin, indium, and their alloys.[36,37] According to the literature, the 6-mercaptopurine (**MP**) drug showed promising corrosion inhibition efficiency for copper metal.[38] Additionally, the bronze layer was protected by the purine derivative thioguanine (**TG**).[39] The experimental findings revealed that the **TG** drug exhibited outstanding anodic and cathodic bifunctional corrosion inhibition performance.[39] A literature survey unveiled that no solid investigation has been systematically proposed to assess the anti-corrosive efficiency of the 6-mercaptopurine (**MP**) and 6-thioguanine (**TG**) drugs on the **Al (111)** surface. In that spirit, the current work is devoted to elucidating the efficacy of the **MP** and **TG** drugs as corrosion inhibitors for the **Al (111)** surface (Fig. 1).

The correlation of the molecular structure with the potentiality of the investigated drugs as corrosion inhibitors was first examined by employing a series of quantum mechanical calculations. Henceforth, molecular dynamics (MD) simulations were conducted for the adsorption process of the **MP** and **TG** drugs on the **Al (111)** surface. Upon obtaining the preferable complexes, the interaction and binding energies were computed. Following that, charge analysis was executed to estimate the role of the charge transfer on the interactions between the investigated inhibitors and the metallic surface. The obtained findings would provide the foundation for utilizing eco-friendly drugs, especially thiopurines, as anti-corrosive inhibitors for the aluminium surface.

2 Computational Methods

2.1. Quantum chemical calculations

DFT computations were carried out for protonated and non-protonated forms of the 6-mercaptopurine (**MP**) and 6-thioguanine (**TG**) drugs in the gas and aqueous phases using the B3LYP/6-311G** level of theory with the help of Gaussian 09 software.[40] The polarizable continuum model was utilized for the computations in the aqueous phase.[41]

Optimization of the geometrical structures of the **MP** and **TG** drugs was first performed. Frequency computations were executed to confirm the true minima for their structures. To elucidate the nucleophilic and electrophilic regions over the surface of the chemical systems, electrostatic potential (ESP) analysis was executed on the optimized compounds. Upon earlier recommendations, an electron density envelope with a value of 0.002 au was devoted to extracting the ESP maps.[42]

To investigate the electronic parameters of the studied thiopurine drugs, FMOs theory was employed. Using FMOs, the electron density distribution of HOMO and LUMO were plotted, and their energies (*i.e.*, E_{HOMO} and E_{LUMO}) were computed. E_{gap} was calculated as the energy difference between E_{LUMO} and E_{HOMO} as follows:

$$E_{gap} = E_{LUMO} - E_{HOMO} \quad (1)$$

Using Koopmans's approximation method, the IP and EA were computed as the negative values of the energies of HOMO and LUMO, respectively, as follows:

$$\text{Koopmans' IP} \approx -E_{HOMO} \quad (2)$$

$$\text{Koopmans' EA} \approx -E_{LUMO} \quad (3)$$

With the incorporation of the energy vertical method, the IP and EA were assessed by utilizing the total electronic energy of the neutral molecule ($E_{Neutral}$) and its corresponding anion ($E^{Anion}_{Neutral}$) and cation ($E^{Cation}_{Neutral}$), obtained from the geometry of the neutral molecule to keep the external potential constant in the fashion of the following equations:

$$\text{Vertical's IP} = E^{\text{Cation}}_{\text{Neutral}} - E_{\text{Neutral}} \quad (4)$$

$$\text{Vertical's EA} = E_{\text{Neutral}} - E^{\text{Anion}}_{\text{Neutral}} \quad (5)$$

Regarding the energy adiabatic method, the IP and EA were calculated upon obtaining the values of the total electronic energy of the optimized geometry of the neutral molecule (E_{Neutral}), anion (E_{Anion}) and cation (E_{Cation}) based on eqn (6) and (7).

$$\text{Adiabatic's IP} = E_{\text{Cation}} - E_{\text{Neutral}} \quad (6)$$

$$\text{Adiabatic's EA} = E_{\text{Neutral}} - E_{\text{Anion}} \quad (7)$$

Upon calculating the values of IP and EA from the above-mentioned methods, the global descriptors of reactivity, including η, σ, π, X, $\Delta E_{\text{Back-donation}}$, ω, and ΔN, were computed as per eqn (8)–(14).

$$\eta = \frac{\text{IP} - \text{EA}}{2} \quad (8)$$

$$\sigma = \frac{1}{\eta} \quad (9)$$

$$\chi = \frac{\text{IP} + \text{EA}}{2} \quad (10)$$

$$\pi = -\chi \quad (11)$$

$$\Delta E_{\text{Back-donation}} = -\frac{\eta}{4} \quad (12)$$

$$\omega = \frac{\Pi^2}{2\eta} \quad (13)$$

$$\Delta N = \frac{[\Phi_{\text{Metal}} - X_{\text{Inhibitor}}]}{2(\eta_{\text{Metal}} + \eta_{\text{Inhibitor}})} \quad (14)$$

The metal work function (Φ_{Metal}), inhibitor electronegativity ($X_{\text{Inhibitor}}$), and metal hardness (η_{Metal}), and inhibitor hardness (η_{Metal}) were involved in eqn (14). Φ_{Metal} and η_{Metal} values were 4.26 eV and 0, respectively.[43–45]

The local reactivity of the investigated drugs was evaluated in terms of the Fukui function indices (*i.e.*, $f_k^+(r)$, $f_k^-(r)$, and $\Delta f(r)$) upon eqn (15)–(17):[46,47]

$$f_k^+(r) = \rho_k(N+1) - \rho_k(N) \quad (15)$$

$$f_k^-(r) = \rho_k(N) - \rho_k(N-1) \quad (16)$$

$$\Delta f(r) = f_k^+(r) - f_k^-(r) \quad (17)$$

For atom k, the charge values of the neutral ($\rho_k(N)$), anionic ($\rho_k(N+1)$), and cationic ($\rho_k(N-1)$) forms were utilized to evaluate the aforesaid indices.

2.2. Molecular dynamics (MD) simulations

Using the Quantum ESPRESSO 6.4.1 package,[48,49] molecular dynamics (MD) simulations in the NVT ensemble at 298 K were performed to investigate the interactions of the **MP** and **TG** drugs with the **Al (111)** surface. According to the experiments and theoretical studies, the **Al (111)** surface has been demonstrated to be the most thermodynamically stable surface.[50] Therefore, the **Al (111)** surface was designed with three layers of aluminium atoms as a periodic slab, setting a 20 Å layer of vacuum along the *z*-axis of the **Al (111)** slab. A 6 × 6 × 1 supercell of **Al (111)**, containing 108 atoms, was then constructed (Fig. 1). Afterwards, the **MP** and **TG** drugs were placed on the **Al (111)** surface to assess their ability toward corrosion inhibition (see Fig. 1).

Generalized Gradient Approximation (GGA) within the Perdew–Burke–Ernzerhof (PBE) exchange-correlation functional was utilized.[51] The electron–ion interactions were described *via* the ultrasoft pseudopotential.[52] The kinetic energy and charge density cutoffs were set to 50 and 500 Ry, respectively. The 10^{-4} eV and 10^{-3} eV Å^{-1} were set to be the energy and force convergences criteria, respectively. In order to sample the first Brillouin zone, the *k*-points of the 2 × 2 × 1 grid were utilized for the geometric optimization and charge transfer computations. The Al atoms in the bottom layer were set to be fixed through the relax calculations, while the two top layers of the slab were fully optimized with the inhibitors. For all calculations, the Marzari–Vanderbilt smearing technique was employed.[53] Grimme's DFT-D2 correction method was considered to represent the long-range van der Waals interactions.[54] The MD calculations were performed at a simulation time of 0.5 ps with a time step (dt) of 0.97 fs and steps number (*n*step) of 1000 steps.

2.3. Interaction and binding energies calculations

Upon the MD simulations, the most stable configurations of the **MP/TG**···**Al (111)** complexes were selected and thoroughly studied. The interaction energies (E_{int}) of the selected complexes were calculated based on the following equation:

$$E_{\text{int}} = E_{\textbf{MP/TG}\cdots\textbf{Al (111)}} - (E_{\textbf{Al (111)}\text{ in complex}} + E_{\textbf{MP/TG}\text{ in complex}}) \quad (18)$$

where $E_{\textbf{MP/TG}\cdots\textbf{Al (111)}}$, $E_{\textbf{Al (111)}\text{ in complex}}$, and $E_{\textbf{MP/TG}\text{ in complex}}$ are the energies of the complex, **Al (111)** surface in complex, and **MP/TG** drugs in complex, respectively. Additionally, the binding energies (E_{bind}) were computed for the investigated complexes as follows:

$$E_{\text{bind}} = E_{\textbf{MP/TG}\cdots\textbf{Al (111)}} - (E_{\text{isolated }\textbf{Al (111)}} + E_{\text{isolated }\textbf{MP/TG}}) \quad (19)$$

where $E_{\textbf{MP/TG}\cdots\textbf{Al (111)}}$, $E_{\text{isolated }\textbf{Al (111)}}$, and $E_{\text{isolated }\textbf{MP/TG}}$ are the energies of the complex, isolated **Al (111)** surface, and isolated adsorbed drugs, respectively. The Bader charge method[55,56] was applied to estimate the charge transfer (Q_t) to or from the **Al (111)** surface using eqn (20):

$$Q_t = Q_{\text{combined }\textbf{Al (111)}} - Q_{\text{isolated }\textbf{Al (111)}} \quad (20)$$

where $Q_{\text{combined }\textbf{Al (111)}}$ and $Q_{\text{isolated }\textbf{Al (111)}}$ are the charges of the combined and isolated **Al (111)** surface, respectively. Charge density difference ($\Delta\rho$) maps were depicted using the following equation:

$$\Delta\rho = \rho_{\mathbf{MP/TG}\cdots\mathbf{Al\ (111)}} - \rho_{\mathbf{Al\ (111)}} - \rho_{\mathbf{MP/TG}} \quad (21)$$

where $\rho_{\mathbf{MP/TG}\cdots\mathbf{Al\ (111)}}$, $\rho_{\mathbf{Al\ (111)}}$, and $\rho_{\mathbf{MP/TG}}$ are the charge densities of the complex, **Al (111)** surface, and **MP**/**TG** drug, respectively. To generate the charge density maps, the VESTA visualization software was used.[57]

For implicit water solvent calculations, the environ code[58] of Quantum ESPRESSO was utilized with a dielectric constant of 78.3. The solvent effect on the interaction energy of the studied complexes was computed according to the following equation:

$$E_{\mathrm{int}}^{\mathrm{solvent\ effect}} = E_{\mathrm{int}}^{\mathrm{water}} - E_{\mathrm{int}}^{\mathrm{gas}} \quad (22)$$

where $E_{\mathrm{int}}^{\mathrm{water}}$ and $E_{\mathrm{int}}^{\mathrm{gas}}$ are the interaction energies of the complex in water and gas media, respectively.

3 Results and discussion

3.1. ESP analysis

Electrostatic potential (ESP) analysis is a dependable tool to provide pictorial evidence for either the nucleophilic or electrophilic nature of the chemical systems three-dimensionally.[59,60] On the optimized structures of the neutral and protonated forms of the **MP** and **TG** drugs, molecular electrostatic potential (MEP) maps were portrayed in the gas and aqueous phases using an electron density envelope with a value of 0.002 au (Fig. 2).

Looking at Fig. 2, electron-rich and -deficient centers were identified within the scouted drugs by red- and blue-colored regions, respectively. Evidently, the most negative potentials over the MEP map of the neutral drugs were observed above the sulfur and nitrogen atoms, reflecting their prominent nucleophilic nature. Notably, a negative ESP was found over the hexagonal ring of the drugs under study in the protonated form more than that in the neutral one. The observed nucleophilic character of the studied inhibitors predicted their potential versatility toward interacting with metallic surfaces (*i.e.*, electrophilic surfaces).

3.2. FMOs analysis

The anti-corrosive efficacy of the **MP** and **TG** drugs was examined using the frontier molecular orbitals (FMOs) theory. From the FMOs, the distributions of the highest occupied molecular orbitals (HOMO) and the lowest unoccupied molecular orbitals (LUMO) distributions were plotted for inhibitory compounds under investigation, and are shown in Fig. 3. Energies of the aforesaid molecular orbitals (*i.e.*, E_{HOMO} and E_{LUMO}) along with their gap E_{gap} were evaluated (Table 1).

As can be seen in Fig. 3, the HOMO levels of the two neutral thiopurine drugs in gas and aqueous phases were denoted surrounding the sulfur atom, while HOMO densities of the protonated thiopurine drugs were distributed around the whole molecules. The LUMO distributions were observed over the two rings of thiopurine drugs in the neutral and protonated molecules (Fig. 3).

According to the literature, E_{HOMO} and E_{LUMO} values describe the potentiality of the chemical systems to donate and accept electrons, respectively. From the literature, chemical systems with less negative E_{HOMO} values showed a more prominent tendency toward giving electrons to the electrophiles that have low energy of unoccupied orbitals.[61,62] It is apparent from Table 1 that the **TG** drug showed higher values of E_{HOMO} (*i.e.*, less negative) than the **MP** drug in all of the studied cases, demonstrating its prominent preferability toward donating electrons. Numerically, the E_{HOMO} values of the neutral form of the **TG** and **MP** drugs in the gas phase were −5.50 and −5.74 eV, respectively. Comparatively, the neutral form of the investigated thiopurine drugs was denoted with higher E_{HOMO} in the gas phase than in the aqueous phase, and the opposite is true in the protonated form. In both gas and aqueous phases, the studied drugs generally showed higher efficiency in the case of the neutral form than the protonated one. The **TG** drug showed less negative E_{LUMO} values than the **MP** drug in the gas and aqueous phases, respectively.

E_{gap} is a descriptive electronic parameter that depends on the reactivity of the inhibitory compound, unveiling its adsorption tendency toward the metallic surface. As E_{gap} decreases (*i.e.*, less positive), the molecular reactivity level is up. In this regard, as listed in Table 1, the **TG** and **MP** drugs had lower E_{gap} values in the neutral form compared with the protonated one.

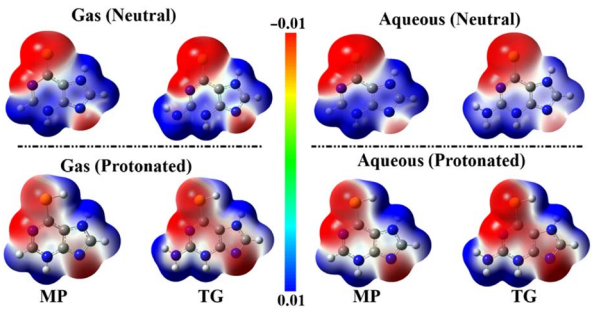

Fig. 2 ESP maps of the 6-mercaptopurine (MP) and 6-thioguanine (TG) drugs.

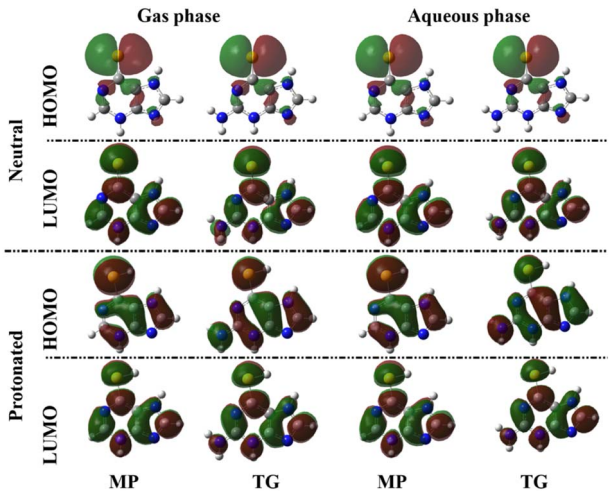

Fig. 3 HOMO and LUMO distributions of the 6-mercaptopurine (MP) and 6-thioguanine (TG) drugs.

Table 1 E_{HOMO}, E_{LUMO}, and E_{gap} of the 6-mercaptopurine (**MP**) and 6-thioguanine (**TG**) drugs in eV

Compound	E_{HOMO}	E_{LUMO}	E_{gap}
Gas (neutral)			
MP	−5.74	−2.06	3.68
TG	−5.50	−1.69	3.81
Gas (protonated)			
MP	−11.53	−6.99	4.54
TG	−10.96	−6.31	4.64
Aqueous (neutral)			
MP	−6.21	−2.17	4.04
TG	−6.07	−1.82	4.25
Aqueous (protonated)			
MP	−7.72	−3.08	4.64
TG	−7.26	−2.64	4.62

3.3. Global reactivity descriptors

To obtain deeper insight into the reactivity of corrosion inhibitors, a wide scope of global reactivity descriptors, including ionization potential (IP), electron affinity (EA), global hardness (η), chemical potential (π), global softness (σ), electronegativity (X), total energy change ($\Delta E_{Back\text{-}Donation}$), electrophilicity ($\omega$), and a number of transferred electrons (ΔN), were evaluated by Koopmans, energy vertical and adiabatic methods (Table 2).

By employing Koopmans' theorem, IP and EA can be computed from the E_{HOMO} and E_{LUMO} energies using eqn (2) and (3), respectively. IP is a basic parameter for the reactivity of a molecule. A high IP means high stability and chemical inertness, and the opposite is true for small IP.[63] As shown in Table 2, the **TG** drug showed lower IP and higher EA values than the **MP** drug. For example, the neutral form of the **TG** and **MP** drugs in the gas phase had Koopmans' IP values of 5.50 and 5.74 eV, respectively.

From the view of the hard and soft acid and bases (HSAB) theory, the inhibitory compound with high softness shows superb corrosion efficiency toward the metallic surfaces, and the opposite is true for the hardness property.[64–66] The inhibitor could be adsorbed onto a metallic surface through the part of a molecule with the lowest hardness and greatest softness.[67] In both gas and aqueous phases, the neutral form of the studied thiopurine drugs exhibited lower η and higher σ values than the protonated one, outlining their notable reactivity and, accordingly, their favorability in the corrosion inhibition process. Quantitatively, the neutral and protonated forms of the **TG** drug in the gas phase had Koopmans' η values of 1.90 and 2.32 eV, respectively. Generally, the drugs understudy in the gas phase showed lower η and higher σ values compared with the aqueous phase. As numerical evidence, the neutral form of the **TG** drug in the gas and aqueous phases had Koopmans' η values of 1.90 and 2.13 eV, respectively.

The HSAB theory documented the χ of a molecule as a crucial reactivity property. The χ difference can reveal the electron flow direction between the inhibitors and the surface of the metal.[68] It has been reported that the χ value is inversely correlated with the inhibition effectiveness. From Table 2, further suitability of the **TG** drug over the **MP** drug toward the corrosion inhibition process was confirmed by the lower positive χ values of the former drug than the posterior one. Obviously, the lower positive χ values were ascribed to the neutral form of the investigated drugs more than the protonated ones, with prominent favorability in the gas phase.

ω allows an assessment of the global electrophilic nature of a chemical system. From the literature, the efficient electrophile and nucleophile are characterized by higher and lower values of ω,[69] respectively. The listed ω values in Table 2 show the more eminent nucleophilic nature of the **TG** drug in all the studied forms and phases compared with the **MP** drug. Numerically, the neutral forms of the **TG** and **MP** drugs in the gas phase exhibited with Koopmans' ω values of 3.39 and 4.13 eV, respectively.

Regarding the ΔN descriptor, a high negative ΔN value indicates the superior preferable inhibition efficiency. For the studied thiopurine drugs, negative ΔN values were obtained, indicating the good inhibition efficiency of the examined drugs.[70] $\Delta E_{Back\text{-}donation}$ is another characteristic property for the chemical reactivity that was adopted to assess the received charge by each of the interacting species within the corrosion inhibition process. The two thiopurine drugs in all cases had negative values of $\Delta E_{Back\text{-}donation}$, outlining the occurrence of the back donation process, which strengthens the adhesion of the inhibitor to the aluminium surface.

Considering the evaluated global reactivity descriptors using Koopmans, energy vertical and adiabatic methods, the three methods exhibited a nearly similar pattern for the neutral and protonated forms of the studied drugs in the gas and aqueous phases.

3.4. Local reactivity: Fukui functions

Toward identifying the plausible nucleophilic and electrophilic regions, local reactivity of the investigated inhibitory compounds was estimated in terms of Fukui function indices. In this regard, nucleophilic ($f_k^+(r)$) and electrophilic ($f_k^-(r)$) Fukui function indices and their difference ($\Delta f(r)$) were computed, and are summarized in Table 3 for all atoms of the studied thiopurine drugs. Fig. S1† displays the plots of the nucleophilic and electrophilic Fukui function indices isosurfaces. As shown in Fig. S1,† the sulfur atom was observed with a higher positive purple-coded region than other atoms, reflecting its prominent suitability for the electrophilic attack. It is proven that the most appropriate regions for the nucleophilic and electrophilic attack were, in conjugation, the regions with the highest $f_k^+(r)$ and $f_k^-(r)$ values.[71,72] High preferability for electrophilic and nucleophilic attacks was perceived for the atoms that possess values more and less than zero, respectively.[73] According to the data gathered in Table 3, sulfur and nitrogen heteroatoms were identified as suitable sites for the electrophilic attack by their higher positive $\Delta f(r)$ values compared with other atoms. In general, sulfur atoms of the **MP** and **TG** drugs were observed with the highest positive $\Delta f(r)$

Table 2 Global reactivity descriptors of 6-mercaptopurine (MP) and 6-thioguanine (TG) drugs

Compound	Method	IP (eV)	EA (eV)	η (eV)	σ (eV^{-1})	π (eV)	χ (eV)	$\Delta E_{\text{Back-donation}}$ (eV)	ω (eV)	ΔN
Gas (neutral)										
MP	Koopmans	5.74	2.06	1.84	0.54	−3.90	3.90	−0.46	4.13	0.10
	Vertical	7.83	0.25	3.79	0.26	−4.04	4.04	−0.95	2.15	0.03
	Adiabatic	7.64	0.39	3.63	0.28	−4.01	4.01	−0.91	2.22	0.03
TG	Koopmans	5.50	1.69	1.90	0.52	−3.59	3.59	−0.48	3.39	0.17
	Vertical	7.57	0.01	3.78	0.26	−3.79	3.79	−0.95	1.90	0.06
	Adiabatic	7.30	0.25	3.53	0.28	−3.78	3.78	−0.88	2.02	0.07
Gas (protonated)										
MP	Koopmans	11.53	6.99	2.27	0.44	−9.26	9.26	−0.57	18.88	−1.10
	Vertical	13.54	5.11	4.22	0.24	−9.32	9.32	−1.05	10.31	−0.60
	Adiabatic	13.42	5.21	4.10	0.24	−9.32	9.32	−1.03	10.57	−0.62
TG	Koopmans	10.96	6.31	2.32	0.43	−8.64	8.64	−0.58	16.06	−0.94
	Vertical	12.82	4.5	4.16	0.24	−8.66	8.66	−1.04	9.01	−0.53
	Adiabatic	12.65	4.67	3.99	0.25	−8.66	8.66	−1.00	9.40	−0.55
Aqueous (neutral)										
MP	Koopmans	6.21	2.17	2.02	0.50	−4.19	4.19	−0.50	4.35	0.02
	Vertical	6.07	2.33	1.87	0.53	−4.20	4.20	−0.47	4.71	0.02
	Adiabatic	5.96	2.45	1.76	0.57	−4.20	4.20	−0.44	5.03	0.02
TG	Koopmans	6.07	1.82	2.13	0.47	−3.94	3.94	−0.53	3.66	0.07
	Vertical	5.93	1.98	1.97	0.51	−3.96	3.96	−0.49	3.96	0.08
	Adiabatic	5.82	2.22	1.80	0.56	−4.02	4.02	−0.45	4.49	0.07
Aqueous (protonated)										
MP	Koopmans	7.72	3.08	2.32	0.43	−5.40	5.40	−0.58	6.28	−0.25
	Vertical	7.67	3.17	2.25	0.44	−5.42	5.42	−0.56	6.52	−0.26
	Adiabatic	7.57	3.28	2.14	0.47	−5.43	5.43	−0.54	6.87	−0.27
TG	Koopmans	7.26	2.64	2.31	0.43	−4.95	4.95	−0.58	5.30	−0.15
	Vertical	7.21	2.75	2.23	0.45	−4.98	4.98	−0.56	5.56	−0.16
	Adiabatic	7.03	3.07	1.98	0.51	−5.05	5.05	−0.50	6.44	−0.20

Table 3 Fukui function indices of S, N, and C atoms of the 6-mercaptopurine (MP) and 6-thioguanine (TG) drugs

		Gas Phase						Aqueous Phase					
		Neutral			Protonated			Neutral			Protonated		
Compound	Atom	$f_k^+(r)$	$f_k^-(r)$	$\Delta f(r)$	$f_k^+(r)$	$f_k^-(r)$	$\Delta f(r)$	$f_k^+(r)$	$f_k^-(r)$	$\Delta f(r)$	$f_k^+(r)$	$f_k^-(r)$	$\Delta f(r)$
MP	S	−0.368	−0.578	0.209	−0.223	−0.387	0.165	−0.344	−0.724	0.380	−0.196	−0.435	0.239
	N	−0.006	0.017	−0.023	−0.007	−0.018	0.011	−0.010	0.009	−0.019	−0.011	−0.022	0.011
	N	−0.027	−0.026	−0.002	−0.044	−0.033	−0.011	−0.039	−0.017	−0.022	−0.050	−0.029	−0.021
	N	−0.042	−0.044	0.002	−0.042	−0.051	0.009	−0.028	−0.020	−0.008	−0.032	−0.032	0.000
	N	−0.020	0.003	−0.022	−0.035	−0.039	0.004	−0.022	−0.008	−0.014	−0.034	−0.037	0.002
	C	0.003	0.004	−0.002	−0.009	−0.069	0.060	−0.015	−0.007	−0.008	−0.025	−0.083	0.057
	C	−0.065	−0.053	−0.012	−0.073	−0.059	−0.014	−0.083	−0.040	−0.043	−0.095	−0.067	−0.028
	C	−0.037	−0.046	0.009	−0.086	0.026	−0.112	−0.090	−0.044	−0.046	−0.130	−0.006	−0.124
	C	−0.099	−0.059	−0.040	−0.103	−0.068	−0.035	−0.104	−0.038	−0.066	−0.113	−0.066	−0.047
	C	−0.093	−0.054	−0.040	−0.094	−0.051	−0.043	−0.106	−0.038	−0.068	−0.110	−0.048	−0.062
TG	S	−0.355	−0.582	0.227	−0.212	−0.246	0.035	−0.328	−0.742	0.414	−0.190	−0.190	0.000
	N	−0.027	−0.023	−0.003	−0.036	−0.037	0.001	−0.031	−0.013	−0.018	−0.038	−0.037	0.000
	N	−0.011	0.017	−0.028	−0.012	−0.019	0.007	−0.016	0.010	−0.027	−0.017	−0.025	0.009
	N	−0.038	−0.042	0.004	−0.038	−0.050	0.013	−0.025	−0.018	−0.006	−0.028	−0.040	0.012
	N	−0.021	0.003	−0.024	−0.050	−0.035	−0.015	−0.036	−0.008	−0.028	−0.054	−0.036	−0.018
	N	−0.033	−0.036	0.003	−0.041	−0.086	0.045	−0.029	−0.015	−0.014	−0.034	−0.099	0.065
	C	0.007	0.012	−0.005	0.005	−0.093	0.097	−0.008	−0.002	−0.007	−0.012	−0.113	0.102
	C	−0.071	−0.052	−0.019	−0.081	−0.058	−0.022	−0.091	−0.037	−0.054	−0.102	−0.079	−0.023
	C	−0.044	−0.044	0.001	−0.090	0.009	−0.099	−0.097	−0.039	−0.058	−0.136	−0.029	−0.107
	C	−0.061	−0.039	−0.022	−0.058	−0.029	−0.029	−0.073	−0.033	−0.040	−0.078	−0.052	−0.026
	C	−0.098	−0.056	−0.042	−0.103	−0.081	−0.022	−0.108	−0.034	−0.073	−0.114	−0.089	−0.024

values, showing their eminent favorability for electrophilic attack (Table 3). For instance, sulfur atoms of the neutral form of the **MP** and **TG** drugs in the aqueous phase showed the highest $\Delta f(r)$ values of 0.380 and 0.414, respectively.

3.5. Molecular dynamics (MD) simulations

The adsorption behavior of the **MP** and **TG** drugs toward the **Al (111)** surface as effective corrosion inhibitors was unveiled utilizing MD simulations. In this respect, the relationship between the total energy of the **MP**⋯ and **TG**⋯**Al (111)** complexes and the corresponding simulation time was elucidated, and is plotted in Fig. 4.

Based on the MD simulations, the most stable configurations of the **MP**⋯ and **TG**⋯**Al (111)** complexes with the highest negative energies were chosen (see Fig. 5). For the most stable configurations, the interaction (E_{int}) and binding (E_{bind}) energies were then computed and are presented in Table 4.

As evident in Fig. 5, S⋯Al covalent bonds were noticed within the relaxed **MP**⋯ and **TG**⋯**Al (111)** complexes with lengths of 2.39 and 2.42 Å, respectively. These lengths were smaller than the entire summation of the vdW radii of the S and Al atoms. According to the data in Table 4, negative values of interaction energies (E_{int}) were observed for the **MP**⋯ and **TG**⋯

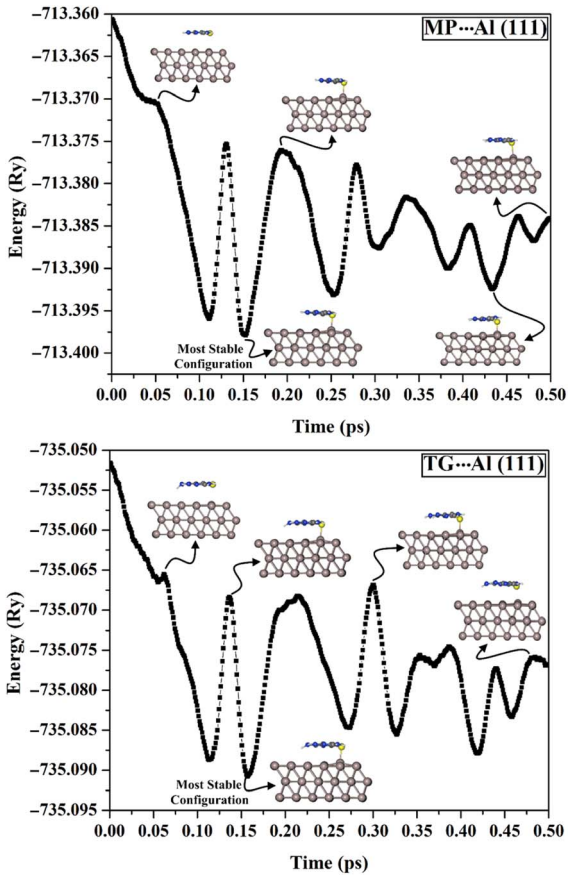

Fig. 4 Correlation between the total energy (in eV) and the molecular dynamics simulation time (in ps) for the 6-mercaptopurine (MP)⋯ and 6-thioguanine (TG)⋯aluminium (Al (111)) complexes.

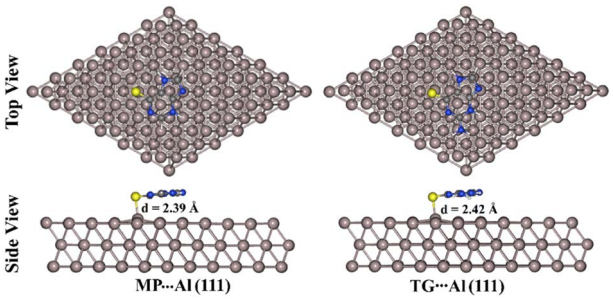

Fig. 5 Top and side representations of the most stable 6-mercaptopurine (MP)⋯ and 6-thioguanine (TG)⋯ aluminium (Al (111)) complexes. The S⋯Al equilibrium distance (d) is in Å.

Al (111) complexes, indicating that the adsorption processes were carried out. The **TG**⋯**Al (111)** complex had higher negative interaction energy than the **MP**⋯**Al (111)** one with values of −1.79 and −1.64 eV, respectively, demonstrating greater efficiency of the corrosion inhibition for the anterior one. The presence of an electron-donating group (*i.e.*, NH_2 group) within the **TG** structure could be the cause of the greater prominence of the molecular inhibitory potency of **TG**.[74]

Considering the structural deformation that occurred during the adsorption process, binding energies (E_{bind}) were estimated (see Table 4). In line with the E_{int} pattern, E_{bind} showed a higher negative value in the case of the **TG**⋯**Al (111)** complex in comparison with the **MP**⋯**Al (111)** counterpart. Numerically, the E_{bind} values of the optimized **TG**⋯ and **MP**⋯**Al (111)** complexes were −1.54 and −1.40 eV, respectively.

Toward a more reliable estimation of the inhibition efficiency, the structures of the most stable configurations of the **MP**⋯ and **TG**⋯**Al (111)** complexes were reoptimized utilizing five layers of **Al (111)** slab (Fig. S1†). Within the relax calculations, the Al atoms in the last two layers were fixed. At the same time, the three top layers of the slab were fully optimized with the inhibitors. E_{int} and E_{bind} were accordingly computed for the relaxed complexes and are listed in Table S1.† According to Fig. S1,† the relaxed **MP**⋯ and **TG**⋯**Al (111)** complexes employing five layers of **Al (111)** slab had interatomic distances that were nearly identical to those in the case of using three layers of **Al (111)** slab. For instance, S⋯Al bond lengths were observed with values of 2.39/2.42 and 2.40/2.42 Å within the relaxed **MP**⋯/**TG**⋯**Al (111)** complexes utilizing three and five layers of **Al (111)** slab, respectively.

Table 4 Interaction (E_{int}, in eV) and binding (E_{bind}, in eV) energies of the most stable 6-mercaptopurine (MP)⋯ and 6-thioguanine (TG)⋯ aluminium (Al (111)) complexes according to the findings of the MD simulations. Interatomic distances (d) are given in Å. Charge transfer (Q_t) values for Al (111) surface following the adsorption of the investigated drugs are calculated in e

System[a]	Bond	d (Å)	E_{int} (eV)	E_{bind} (eV)	Q_t[b] (e)
MP⋯**Al (111)**	S⋯Al	2.39	−1.64	−1.40	−0.67
TG⋯**Al (111)**	S⋯Al	2.42	−1.79	−1.54	−0.52

[a] The most stable configurations are depicted in Fig. 5. [b] Q_t was calculated depending on eqn (20).

From the negative E_{int} and E_{bind} values summarized in Table S1,† the occurrence of the adsorption process was confirmed. Compared to the adsorption process on the surface of the three layers of the **Al (111)** slab, five layers of the **Al (111)** slab showed slightly lower preferability by the energy difference ranging from −0.04 to −0.12 eV. Numerically, the E_{int} values of the adsorbed **MP**/**TG** molecule on three and five layers of the **Al (111)** slab were −1.64/−1.79 and −1.52/−1.75 eV, respectively.

3.6. Electronic properties calculations

The Bader charge analysis is an appropriate method to better understand the transfer of the charge between the adsorbent and the substrate.[55,75] The charge transfer differences (Q_t) of the most stable configurations of the **MP** and **TG** drugs on the surface of **Al (111)** were computed using Bader charge analysis, and the outcomes are summarized in Table 4. Based on the Bader charge findings, the negative values of the Q_t indicate that the charge shifted from the inhibitors to the metallic surface, and the opposite is true for the positive values.

It is clear from Table 4 that the **MP** and **TG** drugs transferred electrons to the **Al (111)** surface *via* the negative Q_t values, indicating that the studied drugs had the potential to interact with the **Al (111)** surface. Such data consequently ensured the potential anti-corrosive activity of the investigated drugs toward the **Al (111)** surface. To gain a better understanding of the adsorption process, the maps of the charge density difference ($\Delta\rho$) for the **MP**⋯ and **TG**⋯**Al (111)** complexes at the most stable configurations were constructed based on eqn (21). The extracted $\Delta\rho$ maps are illustrated in Fig. 6. In the $\Delta\rho$ maps, the sites with increasing and decreasing electron density were detected by colors of yellow and cyan, respectively.

From the data in Table 4, the charge transfer to the **Al (111)** surface from the investigated drugs was indicated by a negative sign of the Q_t values. The amount of the distributed charge on the complexes was in line with the E_{int} findings, at which the **TG**⋯**Al (111)** complex had an E_{int} value that was larger than that of the **MP**⋯**Al (111)** complex.

Looking at Fig. 6, cyan- and yellow-colored regions in the $\Delta\rho$ maps were observed within the **MP**⋯ and **TG**⋯**Al (111)** complexes, indicating the electron gain and loss upon the adsorption process, respectively. Occurrence of charge accumulation (*i.e.*, yellow-colored regions) confirmed the significant affinity of the studied drugs to interact with the surface of **Al (111)** as potential corrosion inhibitors.

To better understand the impact of the adsorption process on the electronic properties of the examined drugs, E_{HOMO}, E_{LUMO}, and E_{gap} values were computed. The data for the studied drugs before and after the adsorption on **Al (111)** surface are listed in Table 5.

From the data in Table 5, notable differences in the E_{HOMO}, E_{LUMO}, and E_{gap} values were observed for the studied drugs before and after the adsorption process. Moreover, the E_{gap} values of **MP** and **TG** drugs were changed after their interaction with the **Al (111)** surface, confirming the occurrence of adsorption processes. For example, the isolated **TG** had an E_{gap} value of 2.284 eV that changed to −0.341 eV after the adsorption process on the **Al (111)** surface (Table 5). Interestingly, the E_{HOMO} values of the isolated drugs decreased after the adsorption on the **Al (111)** surface. For example, the isolated **TG** drug had an E_{HOMO} value of −4.434 eV that decreased to −4.279 eV after the adsorption process on the **Al (111)** surface. The latter observation confirmed the electron-donating property of the **TG** drug, demonstrating that the FMO results were in line with the Bader charge findings (Table 4).

3.7. Solvent effect calculations

To understand the effect of the solvent on the adsorption process within the **MP**/**TG**⋯**Al (111)** complexes, the interaction energy was evaluated in the presence of a water solvent. Afterwards, the solvent effect ($E_{int}^{solvent\ effect}$) energy was calculated for the most preferable configurations as the difference between the interaction energies of the water and gas media (see the Computational Methods section for details). The obtained (E_{int}^{water}) and (E_{int}^{gas}) values are listed in Table 6.

Based on the data in Table 5, the interaction energies of the **MP**/**TG**⋯**Al (111)** complexes in the water medium showed the

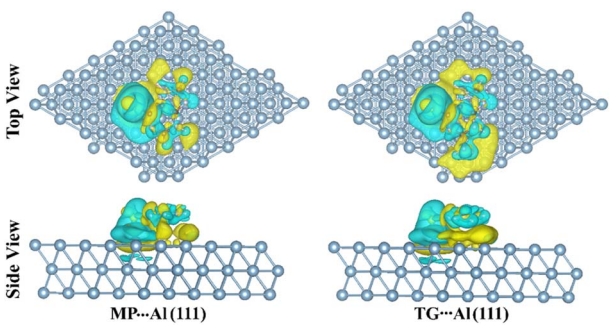

Fig. 6 Top and side views of the charge density difference ($\Delta\rho$) maps of the relaxed structures of the 6-mercaptopurine (MP)⋯ and 6-thioguanine (TG)⋯ aluminium (Al (111)) complexes at the most stable adsorption configurations obtained from the MD simulations. The charge accumulation and depletion were represented by yellow and cyan colors, respectively. The isosurfaces values are in e Å^{-3}.

Table 5 E_{HOMO}, E_{LUMO}, and E_{gap} values for 6-mercaptopurine (MP) and 6-thioguanine (TG) before and after the adsorption process on the Al (111) surface

	E_{HOMO} (eV)	E_{LUMO} (eV)	E_{gap} (eV)
Isolated drug			
MP	−4.681	−2.530	2.151
TG	−4.434	−2.150	2.284
Adsorbed drug			
MP	−4.527	−2.648	1.879
TG	−4.279	−2.231	2.048
Complex[a]			
MP⋯**Al (111)**	0.810	0.470	−0.339
TG⋯**Al (111)**	0.845	0.504	−0.341

[a] Based on the most stable configurations (see Fig. 5).

Table 6 Interaction energies of the most stable 6-mercaptopurine (MP)··· and 6-thioguanine (TG)··· aluminium (Al (111)) complexes in gas (E_{int}^{gas}, in eV), and water (E_{int}^{water}, in eV) media

System[a]	E_{int}^{gas}	E_{int}^{water}	$E_{int}^{solvent\ effect}$
MP···Al (111)	−1.64	−1.23	0.41
TG···Al (111)	−1.79	−1.49	0.30

[a] Based on the most stable configurations (see Fig. 5).

same trend as those in the gas medium. For example, the E_{int} of the **TG···Al (111)** complex was larger than that for the **MP···Al (111)** complex in water, with values of −1.49 and −1.23 eV, respectively (Table 6). Subsequently, the negative values of E_{int} confirmed the occurrence of the adsorption process in the water medium.

4 Conclusions

Herein, detailed insight into the amplitude of the 6-mercaptopurine (**MP**) and 6-thioguanine (**TG**) drugs toward inhibiting the corrosion of the **Al (111)** surface was established using a series of DFT calculations. The ESP findings first showed the prominent nucleophilic nature of the S and N atoms of the examined drugs. Moreover, the FMO results revealed higher values of E_{HOMO} (*i.e.*, less negative) for the **TG** drug than the **MP** drug in all of the studied cases. These higher values demonstrated the greater prominent preferability of the former drug toward donating electrons than the latter one. Generally, the neutral form of the investigated thiopurine drugs had higher E_{HOMO} in the gas phase than in the aqueous phase, and the opposite is true in the protonated form. Using Koopmans, energy vertical and adiabatic methods, the global reactivity descriptors were evaluated, and the higher inhibition efficiency of the **TG** drug over the **MP** analog was generally demonstrated. In summary, the obtained values of the QM descriptors indicated that the **TG** drug showed higher anti-corrosive activity than the **MP** one. In line with the global reactivity affirmations, the nucleophilic and electrophilic Fukui function indices documented a more noticeable preferability of donating electrons in the case of **TG** than **MP**. Consistent with QM descriptors, the interaction energies (E_{int}) confirmed the higher efficiency of the **TG** drug toward inhibiting the corrosion of the **Al (111)** surface than the MP one. E_{int} of **TG···Al (111)** and **MP···Al (111)** complexes showed values up to −1.79 and −1.64 eV, respectively. The energetic results of the solvent effect were in line with the interaction energies in the gas medium that demonstrated a more negative interaction energy for the **TG···Al (111)** complex compared with the **MP···Al (111)** complex. Overall, the above-discussed results are vital for using thiopurine-expired drugs as potential corrosion inhibitors, especially for the **Al (111)** surface.

Author contributions

Conceptualization, Mahmoud A. A. Ibrahim, Tamer Shoeib, and Lamiaa A. Mohamed; methodology, Mahmoud A. A. Ibrahim, Nayra A. M. Moussa, Amna H. M. Mahmoud, Tamer Shoeib, and Lamiaa A. Mohamed; software, Mahmoud A. A. Ibrahim.; formal analysis, Lamiaa A. Mohamed; investigation, Nayra A. M. Moussa, Amna H. M. Mahmoud, and Lamiaa A. Mohamed; resources, Mahmoud A. A. Ibrahim, Shaban R. M. Sayed, and Tamer Shoeib; data curation, Lamiaa A. Mohamed; writing—original draft preparation, Lamiaa A. Mohamed; writing—review and editing, Mahmoud A. A. Ibrahim, Nayra A. M. Moussa, Amna H. M. Mahmoud, Shaban R. M. Sayed, Peter A. Sidhom, Mohamed K. Abd El-Rahman, Tamer Shoeib; visualization, Lamiaa A. Mohamed; supervision, Mahmoud A. A. Ibrahim; project administration, Mahmoud A. A. Ibrahim. All authors have read and agreed to the published version of the manuscript.

Conflicts of interest

There are no conflicts to declare.

Acknowledgements

The authors extend their appreciation to the Researchers Supporting Project number (RSPD2023R743), King Saud University, Riyadh, Saudi Arabia, for funding this work. The computational work was performed with resources provided by the Science and Technology Development Fund (STDF-Egypt, Grants nos. 5480 and 7972), Bibliotheca Alexandrina (**http://hpc.bibalex.org**), and The American University in Cairo. Mahmoud A. A. Ibrahim thanks the Center for High-Performance Computing (CHPC, **http://www.chpc.ac.za**), Cape Town, South Africa, for providing computational resources.

References

1 Y. Otani and S. Sasaki, Effects of the addition of silicon to 7075 aluminum alloy on microstructure, mechanical properties, and selective laser melting processability, *Mater. Sci. Eng., A*, 2020, 777, 139079.
2 A. Heinz, A. Haszler, C. Keidel, S. Moldenhauer, R. Benedictus and W. S. Miller, Recent development in aluminium alloys for aerospace applications, *Mater. Sci. Eng., A*, 2000, **280**(1), 102–107.
3 V. Branzoi, F. Golgovici and F. Branzoi, Aluminium corrosion in hydrochloric acid solutions and the effect of some organic inhibitors, *Mater. Chem. Phys.*, 2003, **78**(1), 122–131.
4 X. H. Liu, Y. Z. Li, L. Lei and X. Wang, The effect of nitrate on the corrosion behavior of 7075-T651 aluminum alloy in the acidic NaCl solution, *Mater. Corros.*, 2021, **72**(9), 1478–1487.
5 C. Luo, S. P. Albu, X. R. Zhou, Z. H. Sun, X. Y. Zhang, Z. H. Tang and G. E. Thompson, Continuous and discontinuous localized corrosion of a 2xxx aluminium-copper-lithium alloy in sodium chloride solution, *J. Alloys Compd.*, 2016, **658**, 61–70.
6 R. Ambat and E. S. Dwarakadasa, Studies on the influence of chloride ion and pH on the electrochemical behaviour of

aluminium alloys 8090 and 2014, *J. Appl. Electrochem.*, 1994, **24**(9), 911–916.

7 A. S. Fouda, F. S. Mohamed and M. W. El-Sherbeni, Corrosion Inhibition of Aluminum–Silicon Alloy in Hydrochloric Acid Solutions Using Carbamidic Thioanhydride Derivatives, *J. Bio- Tribo-Corros.*, 2016, **2**(2), 11.

8 U. Nazir, Z. Akhter, N. Z. Ali and F. U. Shah, Experimental and theoretical insights into the corrosion inhibition activity of novel Schiff bases for aluminum alloy in acidic medium, *RSC Adv.*, 2019, **9**(62), 36455–36470.

9 I. B. Obot, N. O. Obi-Egbedi, S. A. Umoren and E. E. Ebenso, Adsorption and Kinetic Studies on the Inhibition Potential of Fluconazole for the Corrosion of Al in HCl Solution, *Chem. Eng. Commun.*, 2011, **198**(5), 711–725.

10 I. B. Obot and N. O. Obi-Egbedi, Fluconazole as an inhibitor for aluminium corrosion in 0.1M HCl, *Colloids Surf., A*, 2008, **330**(2–3), 207–212.

11 E. E. Oguzie, G. N. Onuoha and E. N. Ejike, Effect of Gongronema latifolium extract on aluminium corrosion in acidic and alkaline media, *Pigment. Resin Technol.*, 2007, **36**(1), 44–49.

12 M. Paz Martínez-Viademonte, S. T. Abrahami, T. Hack, M. Burchardt and H. Terryn, A Review on Anodizing of Aerospace Aluminum Alloys for Corrosion Protection, *Coatings*, 2020, **10**(11), 1106.

13 K. Marcoen, P. Visser, G. F. Trindade, M. L. Abel, J. F. Watts, J. M. C. Mol, H. Terryn and T. Hauffman, Compositional study of a corrosion protective layer formed by leachable lithium salts in a coating defect on AA2024-T3 aluminium alloys, *Prog. Org. Coat.*, 2018, **119**, 65–75.

14 K. Hossam, F. Bouhlal, L. Hermouche, I. Merimi, H. Labjar, A. Chaouiki, N. Labjar, S.-I. Malika, A. Dahrouch, M. Chellouli, B. Hammouti and S. El Hajjaji, Understanding Corrosion Inhibition of C38 Steel in HCl Media by Omeprazole: Insights for Experimental and Computational Studies, *J. Fail. Anal. Prev.*, 2020, **21**(1), 213–227.

15 K. F. Khaled, The inhibition of benzimidazole derivatives on corrosion of iron in 1 M HCl solutions, *Electrochim. Acta*, 2003, **48**(17), 2493–2503.

16 S. M. Elhadi, M. Bilel, B. Abdelmalek and C. Aissa, Experimental evaluation of quinolinium and isoquinolinium derivatives as corrosion inhibitors of mild steel in 0.5 M H2SO4 solution, *Prot. Met. Phys. Chem. Surf.*, 2016, **52**(4), 731–736.

17 H. Ashassi-Sorkhabi, B. Shabani, B. Aligholipour and D. Seifzadeh, The effect of some Schiff bases on the corrosion of aluminum in hydrochloric acid solution, *Appl. Surf. Sci.*, 2006, **252**(12), 4039–4047.

18 M. T. Saeed, M. Saleem, S. Usmani, I. A. Malik, F. A. Al-Shammari and K. M. Deen, Corrosion inhibition of mild steel in 1 M HCl by sweet melon peel extract, *J. King Saud Univ., Sci.*, 2019, **31**(4), 1344–1351.

19 P. B. Raja, M. Ismail, S. Ghoreishiamiri, J. Mirza, M. C. Ismail, S. Kakooei and A. A. Rahim, Reviews on Corrosion Inhibitors: A Short View, *Chem. Eng. Commun.*, 2016, **203**(9), 1145–1156.

20 M. H. O. Ahmed, A. A. Al-Amiery, Y. K. Al-Majedy, A. A. H. Kadhum, A. B. Mohamad and T. S. Gaaz, Synthesis and characterization of a novel organic corrosion inhibitor for mild steel in 1 M hydrochloric acid, *Results Phys.*, 2018, **8**, 728–733.

21 S. K. Ahmed, W. B. Ali and A. A. Khadom, Synthesis and investigations of heterocyclic compounds as corrosion inhibitors for mild steel in hydrochloric acid, *Int. J. Ind. Chem.*, 2019, **10**(2), 159–173.

22 M. A. A. Ibrahim, N. A. M. Moussa, A. H. M. Mahmoud, A. M. Shawky and L. A. Mohamed, On the efficiency of barbituric acid and its thio derivatives as aluminium corrosion inhibitors: A computational study, *J. Mol. Liq.*, 2023, **383**, 122155.

23 K. Tamalmani and H. Husin, Review on Corrosion Inhibitors for Oil and Gas Corrosion Issues, *Appl. Sci.*, 2020, **10**(10), 3389.

24 G. Golestani, M. Shahidi and D. Ghazanfari, Electrochemical evaluation of antibacterial drugs as environment-friendly inhibitors for corrosion of carbon steel in HCl solution, *Appl. Surf. Sci.*, 2014, **308**, 347–362.

25 G. Gece, Drugs: A review of promising novel corrosion inhibitors, *Corros. Sci.*, 2011, **53**(12), 3873–3898.

26 A. A. Nazeer, H. M. El-Abbasy and A. S. Fouda, Antibacterial drugs as environmentally-friendly corrosion inhibitors for carbon steel in acid medium, *Res. Chem. Intermed.*, 2013, **39**(3), 921–939.

27 A. S. Fouda, M. M. Farahat and M. Abdallah, Cephalosporin antibiotics as new corrosion inhibitors for nickel in HCl solution, *Res. Chem. Intermed.*, 2014, **40**(3), 1249–1266.

28 C. Verma, M. A. Quraishi and K. Y. Rhee, Present and emerging trends in using pharmaceutically active compounds as aqueous phase corrosion inhibitors, *J. Mol. Liq.*, 2021, **328**, 115395.

29 N. Vaszilcsin, V. Ordodi and A. Borza, Corrosion inhibitors from expired drugs, *Int. J. Pharm.*, 2012, **431**(1–2), 241–244.

30 M. Scendo, J. Trela and N. Radek, Purine as an effective corrosion inhibitor for stainless steel in chloride acid solutions, *Corros. Rev.*, 2012, **30**(1–2), 33–45.

31 X. H. Li, S. D. Deng, H. Fu and T. H. Li, Adsorption and inhibition effect of 6-benzylaminopurine on cold rolled steel in 1.0 M HCl, *Electrochim. Acta*, 2009, **54**(16), 4089–4098.

32 X. H. Li, S. D. Deng and H. Fu, Synergistic inhibition effect of 6-benzylaminopurine and iodide ion on the corrosion of cold rolled steel in H3PO4 solution, *Corros. Sci.*, 2011, **53**(11), 3704–3711.

33 Y. Yan, W. H. Li, L. K. Cai and B. R. Hou, Electrochemical and quantum chemical study of purines as corrosion inhibitors for mild steel in 1 M HCl solution, *Electrochim. Acta*, 2008, **53**(20), 5953–5960.

34 M. A. Amin, Q. Mohsen and O. A. Hazzazi, Synergistic effect of I− ions on the corrosion inhibition of Al in 1.0M phosphoric acid solutions by purine, *Mater. Chem. Phys.*, 2009, **114**(2–3), 908–914.

35 N. O. Eddy, H. Momoh-Yahaya and E. E. Oguzie, Theoretical and experimental studies on the corrosion inhibition potentials of some purines for aluminum in 0.1 M HCl, *J. Adv. Res.*, 2015, **6**(2), 203–217.

36 A. R. El-Sayed, A. M. Shaker and H. M. A. El-Lateef, Corrosion inhibition of tin, indium and tin-indium alloys by adenine or adenosine in hydrochloric acid solution, *Corros. Sci.*, 2010, **52**(1), 72–81.

37 A.-R. El-Sayed, H. S. Mohran and H. M. Abd El-Lateef, Effect of some nitrogen-heterocyclic compounds on corrosion of tin, indium, and their alloys in HClO4, *Monatsh. Chem.*, 2011, **143**(1), 51–64.

38 F. Alvarez, C. Grillo, P. Schilardi, A. Rubert, G. Benitez, C. Lorente and M. F. de Mele, Decrease in cytotoxicity of copper-based intrauterine devices (IUD) pretreated with 6-mercaptopurine and pterin as biocompatible corrosion inhibitors, *ACS Appl. Mater. Interfaces*, 2013, **5**(2), 249–255.

39 X. Li, A. Feng, Y. Zu, P. Liu, F. Han and M. An, *Electrochemical and Surface Analysis Investigation of Corrosion Inhibition Performance of 6-Thioguanine, Benzotriazole, and Phosphate Salt on Simulated Patinas of Bronze Relics*, DOI: **10.2139/ssrn.4435999**.

40 M. J. Frisch, G. W. Trucks, H. B. Schlegel, G. E. Scuseria, M. A. Robb, J. R. Cheeseman, G. Scalmani, V. Barone, B. Mennucci, G. A. Petersson, H. Nakatsuji, M. Caricato, X. Li, H. P. Hratchian, A. F. Izmaylov, J. Bloino, G. Zheng, J. L. Sonnenberg, M. Hada, M. Ehara, K. Toyota, R. Fukuda, J. Hasegawa, M. Ishida, T. Nakajima, Y. Honda, O. Kitao, H. Nakai, T. Vreven, J. A. Montgomery, J. E. Peralta, F. Ogliaro, M. Bearpark, J. J. Heyd, E. Brothers, K. N. Kudin, V. N. Staroverov, R. Kobayashi, J. Normand, K. Raghavachari, A. Rendell, J. C. Burant, S. S. Iyengar, J. Tomasi, M. Cossi, N. Rega, J. M. Millam, M. Klene, J. E. Knox, J. B. Cross, V. Bakken, C. Adamo, J. Jaramillo, R. Gomperts, R. E. Stratmann, O. Yazyev, A. J. Austin, R. Cammi, C. Pomelli, J. W. Ochterski, R. L. Martin, K. Morokuma, V. G. Zakrzewski, G. A. Voth, P. Salvador, J. J. Dannenberg, S. Dapprich, A. D. Daniels, Ö. Farkas, J. B. Foresman, J. V. Ortiz, J. Cioslowski and D. J. Fox*Gaussian 09, Revision E01; Gaussian09*, Gaussian Inc., Wallingford CT, USA., 2009.

41 J. Tomasi, B. Mennucci and R. Cammi, Quantum mechanical continuum solvation models, *Chem. Rev.*, 2005, **105**(8), 2999–3094.

42 M. A. A. Ibrahim, Molecular mechanical perspective on halogen bonding, *J. Mol. Model.*, 2012, **18**(10), 4625–4638.

43 J. Hölzl, F. K. Schulte and H. Wagner, *Solid Surface Physics*, Springer, 1979, vol. 85.

44 H. B. Michaelson, The work function of the elements and its periodicity, *J. Appl. Phys.*, 1977, **48**(11), 4729–4733.

45 R. Oukhrib, B. El Ibrahimi, H. Abou Oualid, Y. Abdellaoui, S. El Issami, L. Bazzi, M. Hilali and H. Bourzi, In silico investigations of alginate biopolymer on the Fe (110), Cu (111), Al (111) and Sn (001) surfaces in acidic media: Quantum chemical and molecular mechanic calculations, *J. Mol. Liq.*, 2020, **312**, 113479.

46 W. Yang and W. J. Mortier, The use of global and local molecular parameters for the analysis of the gas-phase basicity of amines, *J. Am. Chem. Soc.*, 1986, **108**(19), 5708–5711.

47 K. Fukui, Role of frontier orbitals in chemical reactions, *Science*, 1982, **218**(4574), 747–754.

48 P. Giannozzi, S. Baroni, N. Bonini, M. Calandra, R. Car, C. Cavazzoni, D. Ceresoli, G. L. Chiarotti, M. Cococcioni, I. Dabo, A. Dal Corso, S. de Gironcoli, S. Fabris, G. Fratesi, R. Gebauer, U. Gerstmann, C. Gougoussis, A. Kokalj, M. Lazzeri, L. Martin-Samos, N. Marzari, F. Mauri, R. Mazzarello, S. Paolini, A. Pasquarello, L. Paulatto, C. Sbraccia, S. Scandolo, G. Sclauzero, A. P. Seitsonen, A. Smogunov, P. Umari and R. M. Wentzcovitch, QUANTUM ESPRESSO: a modular and open-source software project for quantum simulations of materials, *J. Phys.: Condens.Matter*, 2009, **21**(39), 395502.

49 P. Giannozzi, O. Andreussi, T. Brumme, O. Bunau, M. Buongiorno Nardelli, M. Calandra, R. Car, C. Cavazzoni, D. Ceresoli, M. Cococcioni, N. Colonna, I. Carnimeo, A. Dal Corso, S. de Gironcoli, P. Delugas, R. A. DiStasio Jr., A. Ferretti, A. Floris, G. Fratesi, G. Fugallo, R. Gebauer, U. Gerstmann, F. Giustino, T. Gorni, J. Jia, M. Kawamura, H. Y. Ko, A. Kokalj, E. Kucukbenli, M. Lazzeri, M. Marsili, N. Marzari, F. Mauri, N. L. Nguyen, H. V. Nguyen, A. Otero-de-la-Roza, L. Paulatto, S. Ponce, D. Rocca, R. Sabatini, B. Santra, M. Schlipf, A. P. Seitsonen, A. Smogunov, I. Timrov, T. Thonhauser, P. Umari, N. Vast, X. Wu and S. Baroni, Advanced capabilities for materials modelling with Quantum ESPRESSO, *J. Phys.: Condens.Matter*, 2017, **29**(46), 465901.

50 Y. Kim and J. Choi, Oxide growth characteristics on Al (100), (110), and (111) surfaces: A chemo-mechanical evaluation, *Mater. Today Commun.*, 2021, **26**, 102006.

51 J. P. Perdew, K. Burke and M. Ernzerhof, Generalized gradient approximation made simple, *Phys. Rev. Lett.*, 1996, **77**(18), 3865–3868.

52 D. Vanderbilt, Soft self-consistent pseudopotentials in a generalized eigenvalue formalism, *Phys. Rev. B*, 1990, **41**(11), 7892–7895.

53 N. Marzari, D. Vanderbilt, A. De Vita and M. C. Payne, Thermal contraction and disordering of the Al(110) surface, *Phys. Rev. Lett.*, 1999, **82**(16), 3296–3299.

54 S. Grimme, Semiempirical GGA-type density functional constructed with a long-range dispersion correction, *J. Comput. Chem.*, 2006, **27**(15), 1787–1799.

55 G. Henkelman, A. Arnaldsson and H. Jonsson, A fast and robust algorithm for Bader decomposition of charge density, *Comput. Mater. Sci.*, 2006, **36**(3), 354–360.

56 W. Kutzelnigg, Book Review: Atoms in Molecules. A Quantum Theory. (International Series Monographs on Chemistry, Vol. 22). By R. F. W. Bader, *Angew. Chem., Int. Ed. Engl.*, 1993, **32**(1), 128–129.

57 K. Momma and F. Izumi, VESTA 3 for three-dimensional visualization of crystal, volumetric and morphology data, *J. Appl. Crystallogr.*, 2011, **44**(6), 1272–1276.

58 O. Andreussi, I. Dabo and N. Marzari, Revised self-consistent continuum solvation in electronic-structure calculations, *J. Chem. Phys.*, 2012, **136**(6), 064102.
59 A. J. Shusterman and L. M. Hoistad, Teaching Chemistry with Electron Density Models. 2. Can Atomic Charges Adequately Explain Electrostatic Potential Maps?, *J. Chem. Educ.*, 2001, **6**(1), 36–40.
60 F. J. Luque, J. M. Lopez and M. Orozco, Perspective on Electrostatic interactions of a solute with a continuum. A direct utilization of *ab initio* molecular potentials for the prevision of solvent effects - Miertus S, Scrocco E, Tomasi J (1981) Chem Phys 55 : 117, *Theor. Chem. Acc.*, 2000, **103**(3–4), 343–345.
61 K. F. Khaled, Electrochemical investigation and modeling of corrosion inhibition of aluminum in molar nitric acid using some sulphur-containing amines, *Corros. Sci.*, 2010, **52**(9), 2905–2916.
62 G. Gece, The use of quantum chemical methods in corrosion inhibitor studies, *Corros. Sci.*, 2008, **50**(11), 2981–2992.
63 Y. Abboud, A. Abourriche, T. Saffaj, M. Berrada, M. Charrouf, A. Bennamara and H. Hannache, A novel azo dye, 8-quinolinol-5-azoantipyrine as corrosion inhibitor for mild steel in acidic media, *Desalination*, 2009, **237**(1–3), 175–189.
64 M. K. Awad, M. R. Mustafa and M. M. A. Elnga, Computational simulation of the molecular structure of some triazoles as inhibitors for the corrosion of metal surface, *J. Mol. Struct.: THEOCHEM*, 2010, **959**(1–3), 66–74.
65 A. Kokalj, On the HSAB based estimate of charge transfer between adsorbates and metal surfaces, *Chem. Phys.*, 2012, **393**(1), 1–12.
66 N. Kovačević and A. Kokalj, Analysis of molecular electronic structure of imidazole- and benzimidazole-based inhibitors: A simple recipe for qualitative estimation of chemical hardness, *Corros. Sci.*, 2011, **53**(3), 909–921.
67 H. Wang, X. Wang, H. Wang, L. Wang and A. Liu, DFT study of new bipyrazole derivatives and their potential activity as corrosion inhibitors, *J. Mol. Model.*, 2007, **13**(1), 147–153.
68 M. Abdallah, A. Al Bahir, H. M. Altass, A. Fawzy, N. El Guesmi, A. S. Al-Gorair, F. Benhiba, I. Warad and A. Zarrouk, Anticorrosion and adsorption performance of expired antibacterial drugs on Sabic iron corrosion in HCl solution: Chemical, electrochemical and theoretical approach, *J. Mol. Liq.*, 2021, **330**, 115702.
69 H. Bourzi, R. Oukhrib, B. El Ibrahimi, H. Abou Oualid, Y. Abdellaoui, B. Balkard, S. El Issami, M. Hilali, L. Bazzi and C. Len, Furfural Analogs as Sustainable Corrosion Inhibitors-Predictive Efficiency Using DFT and Monte Carlo Simulations on the Cu(111), Fe(110), Al(111) and Sn(111) Surfaces in Acid Media, *Sustainability*, 2020, **12**(8), 3304.
70 N. O. Obi-Egbedi, I. B. Obot and M. I. El-Khaiary, Quantum chemical investigation and statistical analysis of the relationship between corrosion inhibition efficiency and molecular structure of xanthene and its derivatives on mild steel in sulphuric acid, *J. Mol. Struct.*, 2011, **1002**(1–3), 86–96.
71 M. E. Belghiti, F. Benhiba, N. Benzbiria, C.-H. Lai, S. Echihi, M. Salah, A. Zeroual, Y. Karzazi, A. Tounsi, K. Abbiche, S. Belaaouad, H. Elalaoui-Elabdallaoui and Y. Naimi, Performance of triazole derivatives as potential corrosion in-hibitors for mild steel in a strong phosphoric acid medium: Combining experimental and computational (DFT, MDs & QSAR) approaches, *J. Mol. Struct.*, 2022, **1256**, 132515.
72 A. El Yaktini, A. Lachiri, M. El Faydy, F. Benhiba, H. Zarrok, M. El Azzouzi, M. Zertoubi, M. Azzi, B. Lakhrissi and A. Zarrouk, Inhibitor effect of new azomethine derivative containing an 8-hydroxyquinoline moiety on corrosion behavior of mild carbon steel in acidic media, *Int. J. Corros. Scale Inhib.*, 2018, **7**(4), 609–632.
73 H. Allal, Y. Belhocine and E. Zouaoui, Computational study of some thiophene derivatives as aluminium corrosion inhibitors, *J. Mol. Liq.*, 2018, **265**, 668–678.
74 A. Singh, K. R. Ansari, M. A. Quraishi and H. Lgaz, Effect of Electron Donating Functional Groups on Corrosion Inhibition of J55 Steel in a Sweet Corrosive Environment: Experimental, Density Functional Theory, and Molecular Dynamic Simulation, *Materials*, 2019, **12**(1), 1–17.
75 R. F. W. Bader and T. T. Nguyen-Dang, Quantum Theory of Atoms in Molecules–Dalton Revisited, in *Advances in Quantum Chemistry*, ed. Löwdin, P.-O., Academic Press, 1981, vol. 14, pp. 63–124.